The effects of orbital precession on tropical precipitation: Mechanisms controlling precipitation changes over land and ocean

Kimberly A. Chamales[1], Amy C. Clement[1], Simona Bordoni[2], and Lisa N. Murphy[1]

[1] Rosenstiel School of Marine and Atmospheric Science, University of Miami, Miami, FL 33149, USA

[2] California Institute of Technology, Pasadena, CA 91125, USA

Corresponding author address: Kimberly Chamales, RSMAS/MPO 4600 Rickenbacker Causeway, Miami, FL 33149, USA. E-mail: kchamales@rsmas.miami.edu

Abstract

The tropical precipitation response to precessional forcing is investigated using idealized precession experiments from the Geophysical Fluid Dynamics Laboratory Coupled Model version 2.1 and mid-Holocene experiments from ten general circulation models participating in the Paleoclimate Modeling Intercomparison Project Phase III. Both sets of experiments show a seasonal land-ocean asymmetry in the tropical precipitation response: precipitation increases over land and decreases over ocean in the season with increased insolation and the opposite is true in the season with decreased insolation. This response is examined using a framework that describes how changes in net top-of-atmosphere radiation affect the atmosphere and surface energy balances. Over land, surface energy storage is small and changes in precipitation are balanced by changes in moist static energy flux divergence. Over ocean, surface energy storage is large, moist static energy flux divergence is small, and changes in precipitation are ultimately driven by changes in circulation and atmospheric stability.

1. Introduction

Earth's orbital variations impact climate over glacial-interglacial timescales by altering the amount of insolation reaching the top of the atmosphere. Orbital precession modulates seasonal insolation and impacts climate on cycles of about 20 kyr. Precessional signals have been observed in a variety of tropical precipitation records including speleothems from Asia and South America [*Cruz et al.*, 2005; *X Wang et al.*, 2006; *X Wang et al.*, 2007; *Y Wang et al.*, 2008] and sediment cores from Asia, South America, and Africa [*Street and Grove*, 1979; *F. Gasse et al.*, 1991; *deMenocal et al.*, 2000; *Françoise Gasse*, 2000; *Bush et al.*, 2002; *Trauth et al.*, 2003; *Herzschuh*, 2006] Paleorecords also provide evidence that intensified monsoon precipitation occurred during the mid-Holocene, a period about 6 ka that was characterized by enhanced insolation due to precessional forcing [*Winkler and Wang*, 1993; *Yu and Harrison*, 1996; *Jolly et al.*, 1998; *Yu et al.*, 1998; *Kohfeld and Harrison*, 2000; *Baker et al.*, 2001; *Haug et al.*, 2001; *Marchant et al.*, 2009]. Understanding the relationship between precessional changes in insolation and precipitation can help explain how precipitation changed in past climates on glacial-interglacial timescales and how it might change in the future.

A variety of modeling studies show that a land-ocean shift in precipitation exists as a result of mid-Holocene forcing [*Braconnot et al.*, 2007; *Braconnot et al.*, 2008; *Hsu et al.*, 2010; *Bosmans et al.*, 2012; *Zhao and Harrison*, 2012] and idealized precessional forcing [*Tuenter et al.*, 2003; *Clement et al.*, 2004]. Here, the term "idealized" refers to experiments that do not correspond to any specific past climates. This land-ocean shift in precipitation was originally described as land and sea breezes caused by differences in the heating of land and ocean [*Kutzbach and Ottobliesner*, 1982; *COHMAP Members*,

1988; *Tuenter et al.*, 2003; *Ruddiman*, 2008; *Bosmans et al.*, 2012]. *Bosmans et al.* [2012] summarize this mechanism and show that increased summer insolation strengthens the thermal low over the warming continents, which increases the land-sea pressure gradient and the monsoon winds. However, *Merlis et al.* [2013a] suggest that changes in precipitation cannot simply be explained through differences in the heating of land and ocean, because changes in the monsoonal circulation are constrained by changes in the atmospheric energy balance rather than by the surface temperature gradient. In an aquaplanet configuration, this can lead to the counterintuitive result of a weaker circulation in the summer with perihelion, despite an increase in the precipitation there [*Merlis et al.*, 2013b]. Hence, *Merlis et al.* [2013a] argue for a more fundamental role of the energetic framework in studies of the tropical precipitation response to radiative perturbations. *Merlis et al.* [2012] develop a framework describing precessional changes in monsoonal circulation in terms of changes in the net top-of-atmosphere (TOA) radiation with idealized aquaplanet simulations, and *Merlis et al.* [2013a] apply the framework to simulations with a zonally symmetric land surface. The purpose of this study is to extend the framework of *Merlis et al.* [2012] and *Merlis et al.* [2013a] to a climate model with a realistic distribution of land and a more complete set of physical processes in order to better understand the tropical hydrological response to precessional forcing.

Hsu et al. [2010] also discusses the land-ocean asymmetry of tropical precipitation changes in the mid-Holocene using an energetic approach similar to the one used by *Merlis et al.* [2013a]. They use a balance of moist static energy (MSE) and radiative fluxes at the TOA and surface to explain changes in precipitation over land and

ocean, and find that the previous season insolation forcing is important for the magnitude of the land-ocean precipitation change; the different heat capacity of land and ocean and the associated slow response time of the ocean allows the insolation forcing of one season to cancel out the insolation forcing of the following season, causing changes in precipitation over ocean to lag the changes in precipitation over land. While this previous-season insolation mechanism accounts for part of the magnitude of the precipitation change, the direct-season insolation is still significant for the presence of the land-ocean contrast. Our study focuses on the mechanism controlling the direct-season response of the precipitation changes. Applying a TOA energetic framework to idealized precession experiments can help elucidate how tropical precipitation changes in response to radiative forcing and highlight the differences in the mechanisms controlling precipitation changes over land and ocean. Using the atmospheric energy budget sidesteps some of the large but canceling terms, such as the convective diabatic heating, that appear in the individual moisture and temperature equations [*Neelin*, 2007]. This approach emphasizes the importance of the net energy input into the atmospheric column and its implications for understanding the precipitation response to changes in the TOA energy.

We also examine the changes in tropical precipitation over land and ocean in the Paleoclimate Modeling Intercomparison Project Phase III (PMIP3) mid-Holocene experiments. Analyzing the previously documented land-ocean asymmetry in a suite of climate models with a standardized experimental design can help assess the robustness of this precipitation signal and motivate the need for a complete mechanistic understanding of precessional changes in precipitation.

Section 2 describes the models and experiments used in this study. In Section 3, we discuss the seasonal precipitation change over land and ocean in the PMIP3 models, while results from the idealized experiments and mechanisms used to constrain precipitation changes over land and ocean are examined in Section 4. A brief discussion follows in Section 5.

2. Methodology

We use two sets of experiments for this study. The first is from PMIP3, a project that aims to coordinate paleoclimate modeling and model evaluation using standardized experiments from various models and research institutions across the globe. Here, we use climatological monthly data from the PMIP3 mid-Holocene and pre-industrial control experiments. Table 1 lists the 10 models used in this study, the model years used to compute each climatology, and the reference for each model.

We use mid-Holocene experiments (MH) in which the autumnal equinox is set close to perihelion ($\omega-180=0.87$, where ω is the longitude of perihelion), and preindustrial control experiments (PI) in which the Northern Hemisphere (NH) winter solstice occurs near perihelion ($\omega-180=102.04$). Further details of the forcings and boundary conditions can be found on the PMIP3 website (https://pmip3.lsce.ipsl.fr/). Although there are slight variations in the greenhouse gas concentrations prescribed for MH and PI, the changes resulting from those forcings are small compared to those resulting from the orbital forcing [*Bosmans et al.*, 2012]. We examine the multi-model mean of the difference in the monthly climatologies between the two experiments (MH-PI).

To examine in more detail the mechanisms controlling the precession-induced shift in precipitation between land and ocean, we use idealized simulations from the Geophysical Fluid Dynamics Laboratory (GFDL) Coupled Model version 2.1 (CM2.1). The atmosphere and land components have a horizontal resolution of 2° latitude x 2.5° longitude, and the atmosphere has 24 vertical levels. The ocean model has a horizontal resolution of 1° latitude x 1° longitude – with a latitudinal resolution that gradually decreases equatorward of 30° so that it is 1/3° at the equator – and 50 vertical levels [*Delworth et al.*, 2006].

We use two experiments in which the precessional signal is stronger than in the mid-Holocene experiments. In the first experiment (hereafter referred to as the summer solstice experiment "SS"), perihelion is set at the NH summer solstice (ω–180=270) and in the second experiment (hereafter referred to as the winter solstice experiment "WS"), perihelion is set at the NH winter solstice (ω–180=90). Because eccentricity modulates the strength of precessional forcing [*Jackson and Broccoli*, 2003], eccentricity is increased to 0.0493 in order to maximize the model's response to the precessional forcing. All other parameters are set to pre-industrial levels. A complete description of the experimental design can be found in *Erb et al.* [2013]. The simulations were run for 600 years of which we examine the last 100 years and compute the monthly mean climate changes between the two experiments (SS-WS).

3. Precipitation Changes During the Mid-Holocene

It is of interest to first determine if today's climate models show a robust precipitation signal over land and ocean in response to changes in orbital precession. We

153 do this by examining the multi-model mean seasonal cycle of precipitation change over
154 tropical land and ocean in the PMIP3 models (Fig. 1). In boreal summer, the precipitation
155 change is positive over land and negative over ocean, indicating that the season with
156 enhanced insolation also receives enhanced precipitation over land. The opposite is true
157 in boreal winter: the earth receives less insolation, and the change in precipitation is
158 negative over land and positive over ocean. This result shows that ten of the climate
159 models that participated in PMIP3 respond with a robust land-ocean shift in precipitation,
160 reinforcing the importance of understanding the mechanisms that drive this distinct
161 precipitation signal.
162
163 **4. Precipitation Changes in Idealized Experiments**
164 **4.1. TOA Energetic Mechanism**
165 We now adopt the energetic framework used by *Merlis et al.* [2013a] who
166 constrained the response of the monsoonal Hadley circulation to precessional forcing
167 with an energy budget at the TOA. Their framework was applied to idealized model
168 simulations with a zonally symmetric continent. Here, we extend this framework to
169 GFDL-CM2.1, which has a realistic land configuration.
170 From *Merlis et al.* [2013a], the energy balance of the atmosphere and surface is
171 $$\left\{\frac{\partial \bar{E}}{\partial t}\right\} + \rho_o c_{po} d \frac{\partial \overline{T_s}}{\partial t} = S_{TOA} - L_{TOA} - \nabla \cdot \left\{\overline{\boldsymbol{v}\boldsymbol{h}}\right\} - \nabla \cdot F_o, \quad (1)$$
172
173 where the time-mean is denoted by $\overline{(\cdot)}$ and the vertically mass-weighted integral is
174 denoted by $\{\cdot\}$. $E = c_v T + gz + Lq$ is the total atmospheric energy and $\boldsymbol{h} = c_p T + gz +$
175 Lq is the MSE. S_{TOA} is the net TOA shortwave radiation, L_{TOA} is the net TOA longwave

radiation, ρ_o is the ocean density, c_{po} is the ocean heat capacity, d is the mixed layer depth, T_s is the surface temperature, $\nabla \cdot F_o$ is the ocean energy flux divergence, and $\nabla \cdot \{\overline{\boldsymbol{v}h}\}$ is the atmospheric MSE flux divergence, where $\boldsymbol{v}$ is the horizontal winds. If atmospheric and land energy storage are considered negligible, the balance in (1) becomes

$$S_{TOA} - L_{TOA} \approx A\rho_o c_{po} d \frac{\partial \overline{T_s}}{\partial t} + \nabla \cdot \{\overline{\boldsymbol{v}h}\} + \nabla \cdot F_o, \quad (2)$$

where

$$A = \begin{cases} 1 & \text{over ocean} \\ 0 & \text{over land.} \end{cases}$$

If we consider insolation changes, the perturbation energy balance becomes

$$\delta(S_{TOA} - L_{TOA}) \approx A\rho_o c_{po} d\delta \frac{\partial \overline{T_s}}{\partial t} + \delta\nabla \cdot \{\overline{\boldsymbol{v}h}\} + \delta\nabla \cdot F_o. \quad (3)$$

Over land, the surface storage term and the ocean energy flux divergence are zero, so changes in the net (shortwave minus longwave) TOA radiation are balanced solely by changes in MSE flux divergence. Over ocean, changes in net TOA radiation can be balanced by changes in MSE flux divergence, ocean energy flux divergence, and surface energy storage.

While Eq. (3) is useful because it describes the energy balance of the atmosphere and the surface, it does not explicitly account for changes in precipitation. In order to understand how changes in net TOA radiation lead to changes in precipitation, we link the energy and moisture budgets by considering the atmosphere in equilibrium. The surface warms through radiative heating and convection heats the upper atmosphere

through precipitation and latent heat release. Therefore, in monsoon regions where sufficient surface moisture is available, changes in net TOA radiation over land are balanced by changes in precipitation:

$$\delta P_L \approx \delta(S_{TOA} - L_{TOA}) \approx \delta \nabla \cdot \{\overline{\boldsymbol{v}h}\}, \quad (4)$$

where P_L is the precipitation over land.

4.2. Results

Similar to the mid-Holocene experiments, a land-ocean asymmetry in precipitation exists as a result of the idealized precessional forcing in the GFDL-CM2.1 simulations (Fig. 2). In order to examine the mechanism driving this precipitation signal, we examine the tropical-mean changes in net TOA radiation, net surface fluxes, and MSE flux divergence over land and ocean for both models. As expected from Eqs. (3) and (4), changes in precipitation have the same sign as the changes in net TOA radiation over land surfaces. Energy is redistributed from the surface to the atmosphere through vertical motion, which results in convection and latent heat release. Therefore, over land, increases in net TOA radiation correspond to increases in precipitation and decreases in net TOA radiation correspond to decreases in precipitation.

Over ocean, the sign of the change in net TOA radiative forcing is the same as it is over land, but the change in precipitation is opposite. This difference arises as a result of the ocean energy storage: Fig. 2 indicates that over ocean, changes in net TOA radiation are almost entirely balanced by changes in the surface energy fluxes. The surface storage term dominates over the ocean heat flux divergence term (not shown)

indicating that the energy flux is warming or cooling the ocean surface. The ocean responds to the increase in net TOA radiation during boreal summer by absorbing energy and warming the surface, and it responds to the decrease in net TOA radiation during boreal winter by releasing energy and cooling the surface. As a result, the change in MSE flux divergence over ocean is very small; the atmosphere over ocean does much less work to adjust to the TOA forcing than the atmosphere over land.

While this analysis is useful for understanding the atmospheric energy budget over both land and ocean, it does not explicitly explain why precipitation decreases over ocean when net TOA radiation is increasing, and vice versa. To further understand the oceanic precipitation response, we examine the seasonal cycle of the moisture flux divergence over ocean.

As in *Clement et al.* [2004], we decompose the moisture flux convergence into the effects of the circulation changes, $-\nabla \cdot \{\boldsymbol{v}'\overline{q}\}$, and the effects of the moisture changes, $-\nabla \cdot \{\overline{\boldsymbol{v}}q'\}$, where q is the specific humidity, $\overline{(\cdot)}$ denotes the mean (WS) field and $(\cdot)'$ denotes a deviation from the mean. Fig. 3 shows the change in the seasonal cycle of these terms over ocean. It is evident that the seasonal change in circulation, i.e., the dynamic component, dominates the seasonal change in the specific humidity, i.e., the thermodynamic component (this also true over land, not shown). The effect of the circulation change is such that moisture is diverging over ocean in boreal summer and converging over ocean in boreal winter. This is consistent with the change in precipitation over ocean. We deduce from Fig. 3 that a dynamic mechanism is controlling precipitation changes over ocean (i.e., subsidence and decreased precipitation during boreal summer and ascent and increased precipitation during boreal winter). This differs

243 from the mechanism controlling precipitation changes over land, which is dictated by the
244 atmospheric energy response to a change in net TOA radiation.

245 The thermodynamic structure of the atmosphere may be necessary to explain how
246 precipitation can change over ocean despite little change in the MSE flux divergence.
247 Fig. 4 shows the change in the vertical profiles of the dry and latent energy over land and
248 ocean in boreal winter (DJF) and boreal summer (JJA). The dry energy is taken as $c_p\theta$,
249 where θ is the potential temperature and c_p is the specific heat for dry air, and latent
250 energy is taken as $L_v q$, where L_v is the latent heat of vaporization. The latent energy is
251 most important in the lower levels of the troposphere, and it decreases during DJF when
252 the surface is cooling and increases in JJA when the surface is warming. The profile of
253 $c_p\theta$ has small seasonal change over land and a larger change over ocean. Here, the
254 atmosphere becomes more unstable ($d\theta/dp > 0$) in DJF and more stable ($d\theta/dp < 0$) in
255 JJA.

256 We suggest that a reorganization of the thermodynamic structure of the
257 atmosphere over ocean, which is driven by circulation changes over land, may ultimately
258 allow for a change in precipitation. For example, in boreal summer when there is a net
259 gain in the TOA radiation, the atmosphere over land responds to this forcing through an
260 export of MSE, which is achieved through anomalous vertical motion and an increase in
261 precipitation. It is this circulation change over land that drives anomalous descent over
262 ocean. As we saw in the previous section, the atmosphere over ocean does not import
263 more energy; it may instead adjust by becoming more stable, consistent with less rainfall
264 over ocean.
265

5. Discussion

We examined the precipitation response to mid-Holocene and idealized precessional forcing using a variety of climate models. All models agree that a land-ocean shift in precipitation exists as a result of precessional forcing. The idealized simulations were used to examine the mechanisms controlling this distinct precipitation response. We found that while the TOA energetic mechanism outlined in *Merlis et al.* [2013a] explains how precipitation over land responds to precessional forcing, it does not fully explain the precipitation response over ocean.

The fundamental constraint dictating the energy balance and resulting precipitation change over land and ocean lies in the surface boundary condition. Over land, the surface stores very little energy and the atmosphere is required to do all the work to compensate for the net TOA energy imbalance. We see this in the MSE flux divergence: as the net TOA radiation increases, the atmosphere responds by diverging MSE and latent heat is released through an increase in precipitation, and as net TOA radiation decreases, the atmosphere converges MSE to maintain equilibrium and precipitation decreases. Over ocean, the energy balance is not so simple because surface energy storage plays an important role in balancing the TOA energy fluxes. When the net TOA radiation increases over ocean, the surface warms and the change in MSE flux divergence does not need to be as large as it is over land. When there is a decrease in the net TOA radiation, the ocean surface cools and, again, the change in MSE flux divergence over ocean is small. Therefore, it is the differing surface properties of the land and ocean that allow for very different atmospheric responses to precessional forcing.

While these changes in the energy budgets of the atmosphere and surface are useful for understanding the precipitation response to precessional forcing over land, they do not explicitly explain the land-ocean asymmetry. Analyses of the change in moisture flux convergence and the dry and latent vertical energy profiles of the atmosphere suggest that the atmospheric energy response over land may drive changes in circulation that affect the thermodynamic structure over ocean, allowing for changes in precipitation to occur.

Further insight into this mechanism for describing precipitation changes may provide more details of the climate response to precession than mechanisms traditionally invoked in monsoon dynamics. Understanding the mechanisms that drive changes in precipitation due to precessional forcing can not only help explain precipitation changes in past and future climates, but it can also help explain how the precipitation signal manifests in regional climate records. Moreover, it is of interest to examine regional precipitation changes because over glacial-interglacial timescales, the regional response to solar forcing may differ significantly from the global response [*Clement et al.*, 2004]. This has important implications for the interpretation of climate records and for regional climate sensitivity.

Acknowledgements

We would like to thank Michael Erb and Tony Broccoli for providing the data for the GFDL-CM2.1 idealized simulations. Data is available from K.A.C. upon request and additionally, the PMIP3 data can be found online at http://pcmdi9.llnl.gov/esgf-web-fe/. This study was supported by the National Science Foundation Paleo Perspectives on Climate Change program.

311 **References**

312 Baker, P. A., G. O. Seltzer, S. C. Fritz, R. B. Dunbar, M. J. Grove, P. M. Tapia, S. L.
313 Cross, H. D. Rowe, and J. P. Broda (2001), The history of South American
314 tropical precipitation for the past 25,000 years, *Science*, *291*(5504), 640-643,
315 doi:10.1126/science.291.5504.640.

316 Bao, Q., et al. (2013), The Flexible Global Ocean-Atmosphere-Land system model,
317 Spectral Version 2: FGOALS-s2, *Advances in Atmospheric Sciences*, *30*(3), 561-
318 576, doi:10.1007/s00376-012-2113-9.

319 Bosmans, J. H. C., S. S. Drijfhout, E. Tuenter, L. J. Lourens, F. J. Hilgen, and S. L.
320 Weber (2012), Monsoonal response to mid-holocene orbital forcing in a high
321 resolution GCM, *Climate of the Past*, *8*(2), 723-740, doi:10.5194/cp-8-723-2012.

322 Braconnot, P., C. Marzin, L. Gre´goire, E. Mosquet, and O. Marti (2008), Monsoon
323 response to changes in Earth's orbital parameters: comparisons between
324 simulations of the Eemian and of the Holocene, *Climate of the Past*, *4*, 281–294.

325 Braconnot, P., et al. (2007), Results of PMIP2 coupled simulations of the Mid-Holocene
326 and Last Glacial Maximum - Part 1: experiments and large-scale features, *Climate*
327 *of the Past*, *3*(2), 261-277.

328 Bush, M. B., M. C. Miller, P. E. De Oliveira, and P. A. Colinvaux (2002), Orbital forcing
329 signal in sediments of two Amazonian lakes, *Journal of Paleolimnology*, *27*, 341–
330 352.

331 Clement, A. C., A. Hall, and A. J. Broccoli (2004), The importance of precessional
332 signals in the tropical climate, *Climate Dynamics*, *22*(4), 327-341,
333 doi:10.1007/s00382-003-0375-8.

334 COHMAP Members (1988), Climatic changes of the last 18,000 years: Observations and
335 model simulations, *Science*, *241*(4869), 1043-1052,
336 doi:10.1126/science.241.4869.1043.
337 Cruz, F. W., S. J. Burns, I. Karmann, W. D. Sharp, M. Vuille, A. O. Cardoso, J. A.
338 Ferrari, P. L. S. Dias, and O. Viana (2005), Insolation-driven changes in
339 atmospheric circulation over the past 116,000 years in subtropical Brazil, *Nature*,
340 *434*(7029), 63-66, doi:10.1038/nature03365.
341 Delworth, T. L., et al. (2006), GFDL's CM2 global coupled climate models. Part I:
342 Formulation and simulation characteristics, *Journal of Climate*, *19*(5), 643-674,
343 doi:10.1175/jcli3629.1.
344 deMenocal, P., J. Ortiz, T. Guilderson, J. Adkins, M. Sarnthein, L. Baker, and M.
345 Yarusinsky (2000), Abrupt onset and termination of the African Humid Period:
346 rapid climate responses to gradual insolation forcing, *Quaternary Science*
347 *Reviews*, *19*(1-5), 347-361, doi:10.1016/s0277-3791(99)00081-5.
348 Dufresne, J. L., et al. (2013), Climate change projections using the IPSL-CM5 Earth
349 System Model: from CMIP3 to CMIP5, *Climate Dynamics*, *40*(9-10), 2123-2165,
350 doi:10.1007/s00382-012-1636-1.
351 Erb, M. P., A. J. Broccoli, and A. C. Clement (2013), The contribution of radiative
352 feedbacks to orbitally driven climate change, *Journal of Climate*, *26*(16), 5897-
353 5914, doi:10.1175/jcli-d-12-00419.1.
354 Gasse, F. (2000), Hydrological changes in the African tropics since the Last Glacial
355 Maximum, *Quaternary Science Reviews*, *19*(1–5), 189-211, doi:10.1016/S0277-
356 3791(99)00061-X.

Gasse, F., et al. (1991), A 13,000-year climate record from Western Tibet, *Nature*, *353*(6346), 742-745, doi:10.1038/353742a0.

Gent, P. R., et al. (2011), The Community Climate System Model Version 4, *Journal of Climate*, *24*(19), 4973-4991, doi:10.1175/2011jcli4083.1.

Giorgetta, M. A., et al. (2013), Climate and carbon cycle changes from 1850 to 2100 in MPI-ESM simulations for the Coupled Model Intercomparison Project phase 5, *Journal of Advances in Modeling Earth Systems*, *5*(3), 572-597, doi:10.1002/jame.20038.

Haug, G. H., K. A. Hughen, D. M. Sigman, L. C. Peterson, and U. Rohl (2001), Southward migration of the intertropical convergence zone through the Holocene, *Science*, *293*(5533), 1304-1308, doi:10.1126/science.1059725.

Herzschuh, U. (2006), Palaeo-moisture evolution in monsoonal Central Asia during the last 50,000 years, *Quaternary Science Reviews*, *25*(1-2), 163-178, doi:10.1016/j.quascirev.2005.02.006.

Hsu, Y.-H., C. Chou, and K.-Y. Wei (2010), Land–ocean asymmetry of tropical precipitation changes in the Mid-Holocene, *Journal of Climate*, *23*(15), 4133-4151, doi:10.1175/2010jcli3392.1.

Jackson, C. S., and A. J. Broccoli (2003), Orbital forcing of Arctic climate: mechanisms of climate response and implications for continental glaciation, *Climate Dynamics*, *21*(7-8), 539-557, doi:10.1007/s00382-003-0351-3.

Jolly, D., et al. (1998), Biome reconstruction from pollen and plant macrofossil data for Africa and the Arabian peninsula at 0 and 6000 years, *Journal of Biogeography*, *25*(6), 1007-1027, doi:10.1046/j.1365-2699.1998.00238.x.

Kohfeld, K. E., and S. P. Harrison (2000), How well can we simulate past climates? Evaluating the models using global palaeoenvironmental datasets, *Quaternary Science Reviews*, *19*(1-5), 321-346, doi:10.1016/s0277-3791(99)00068-2.

Kutzbach, J. E., and B. L. Ottobliesner (1982), The sensitivity of the African-Asian monsoonal climate to orbital parameter changes for 9,000 years BP in a low-resolution general-circulation model, *Journal of the Atmospheric Sciences*, *39*(6), 1177-1188, doi:10.1175/1520-0469(1982)039<1177:tsotaa>2.0.co;2.

Li, L. J., et al. (2013), The flexible global ocean-atmosphere-land system model, Grid-point Version 2: FGOALS-g2, *Advances in Atmospheric Sciences*, *30*(3), 543-560, doi:10.1007/s00376-012-2140-6.

Marchant, R., et al. (2009), Pollen-based biome reconstructions for Latin America at 0, 6000 and 18 000 radiocarbon years ago, *Climate of the Past*, *5*(4), 725-767.

Merlis, T. M., T. Schneider, S. Bordoni, and I. Eisenman (2012), Hadley circulation response to orbital precession. Part I: Aquaplanets, *Journal of Climate*, *26*(3), 740-753, doi:10.1175/JCLI-D-11-00716.1.

Merlis, T. M., T. Schneider, S. Bordoni, and I. Eisenman (2013a), Hadley circulation response to orbital precession. Part II: Subtropical continent, *Journal of Climate*, *26*(3), 754-771, doi:10.1175/jcli-d-12-00149.1.

Merlis, T. M., T. Schneider, S. Bordoni, and I. Eisenman (2013b), The tropical precipitation response to orbital precession, *Journal of Climate*, *26*(6), 2010-2021, doi:10.1175/jcli-d-12-00186.1.

Neelin, J. D. (2007), Moist dynamics of tropical convection zones in monsoons, teleconnections and global warming, in *The Global Circulation of the*

403 *Atmosphere*, edited by T. Schneider and A. Sobel, p. 385, Princeton University
404 Press, Princeton.
405 Phipps, S. J., L. D. Rotstayn, H. B. Gordon, J. L. Roberts, A. C. Hirst, and W. F. Budd
406 (2011), The CSIRO Mk3L climate system model version 1.0-Part 1: Description
407 and evaluation, *Geoscientific Model Development*, *4*(2), 483-509,
408 doi:10.5194/gmd-4-483-2011.
409 Ruddiman, W. F. (2008), *Earth's Climate: Past and Future*, 2nd ed., W. H. Freeman &
410 Company.
411 Schmidt, G. A., et al. (2014), Configuration and assessment of the GISS ModelE2
412 contributions to the CMIP5 archive, *Journal of Advances in Modeling Earth*
413 *Systems*, *6*(1), 141-184, doi:10.1002/2013ms000265.
414 Street, F. A., and A. T. Grove (1979), Global maps of lake-level fluctuations since 30,000
415 yr BP, *Quaternary Research*, *12*(1), 83-118, doi:10.1016/0033-5894(79)90092-9.
416 Trauth, M. H., A. L. Deino, A. G. N. Bergner, and M. R. Strecker (2003), East African
417 climate change and orbital forcing during the last 175 kyr BP, *Earth and*
418 *Planetary Science Letters*, *206*(3-4), 297-313, doi:10.1016/s0012-821x(02)01105-
419 6.
420 Tuenter, E., S. L. Weber, F. J. Hilgen, and L. J. Lourens (2003), The response of the
421 African summer monsoon to remote and local forcing due to precession and
422 obliquity, *Global and Planetary Change*, *36*(4), 219-235, doi:10.1016/s0921-
423 8181(02)00196-0.

Voldoire, A., et al. (2013), The CNRM-CM5.1 global climate model: description and basic evaluation, *Climate Dynamics*, *40*(9-10), 2091-2121, doi:10.1007/s00382-011-1259-y.

Wang, X., A. S. Auler, R. L. Edwards, H. Cheng, E. Ito, and M. Solheid (2006), Interhemispheric anti-phasing of rainfall during the last glacial period, *Quaternary Science Reviews*, *25*(23-24), 3391-3403, doi:10.1016/j.quascirev.2006.02.009.

Wang, X., A. S. Auler, R. L. Edwards, H. Cheng, E. Ito, Y. Wang, X. Kong, and M. Solheid (2007), Millennial-scale precipitation changes in southern Brazil over the past 90,000 years, *Geophysical Research Letters*, *34*(23), doi:10.1029/2007gl031149.

Wang, Y., H. Cheng, R. L. Edwards, X. Kong, X. Shao, S. Chen, J. Wu, X. Jiang, X. Wang, and Z. An (2008), Millennial- and orbital-scale changes in the East Asian monsoon over the past 224,000 years, *Nature*, *451*(7182), 1090-1093, doi:10.1038/nature06692.

Watanabe, S., et al. (2011), MIROC-ESM 2010: Model description and basic results of CMIP5-20c3m experiments, *Geoscientific Model Development*, *4*(4), 845-872, doi:10.5194/gmd-4-845-2011.

Winkler, M. G., and P. K. Wang (1993), The Late-Quaternary Vegetation and Climate of China, in *Global Climates Since the Last Glacial Maximum*, edited by H. E. Wright, J. E. Kutzbach, T. Webb III, W. F. Ruddiman, F. A. Street-Perrott and P. J. Bartlein, pp. 221-261, University of Minnesota Press, Minneapolis.

Yu, G., and S. P. Harrison (1996), An evaluation of the simulated water balance of Eurasia and northern Africa at 6000 y BP using lake status data, *Climate Dynamics*, *12*(11), 723-735, doi:10.1007/s003820050139.

Yu, G., I. C. Prentice, S. P. Harrison, and X. J. Sun (1998), Pollen-based biome reconstructions for China at 0 and 6000 years, *Journal of Biogeography*, *25*(6), 1055-1069, doi:10.1046/j.1365-2699.1998.00237.x.

Yukimoto, S., et al. (2012), A new global climate model of the Meteorological Research Institute: MRI-CGCM3-Model description and basic performance, *Journal of the Meteorological Society of Japan*, *90A*, 23-64, doi:10.2151/jmsj.2012-A02.

Zhao, Y., and S. P. Harrison (2012), Mid-Holocene monsoons: a multi-model analysis of the inter-hemispheric differences in the responses to orbital forcing and ocean feedbacks, *Climate Dynamics*, *39*, 1457–1487, doi:10.1007/s00382-011-1193-z.

	Model Years for Climatology		
Model Name	MH	PI	Reference
CCSM4	1000-1300	250-1300	*Gent et al.* [2011]
CNRM-CM5	1950-2149	1850-2699	*Voldoire et al.* [2013]
CSIRO-Mk3L-1-2	1-500	1-1000	*Phipps et al.* [2011]
FGOALS-g2	340-1024	201-900	*Li et al.* [2013]
FGOALS-s2	1-100	1850-2350	*Bao et al.* [2013]
GISS-E2-R	2500-2599	3331-4530	*Schmidt et al.* [2014]
IPSL-CM5A-LR	2301-2800	1800-2799	*Dufresne et al.* [2013]
MIROC-ESM	2330-2429	1800-2429	*Watanabe et al.* [2011]
MPI-ESM-P	1850-1949	1850-3005	*Giorgetta et al.* [2013]
MRI-CGCM3	1951-2050	1851-2350	*Yukimoto et al.* [2012]

458 Table 1. PMIP3 models used in this analysis, model years averaged over for the mid-
459 Holocene and pre-industrial climatologies, and references.

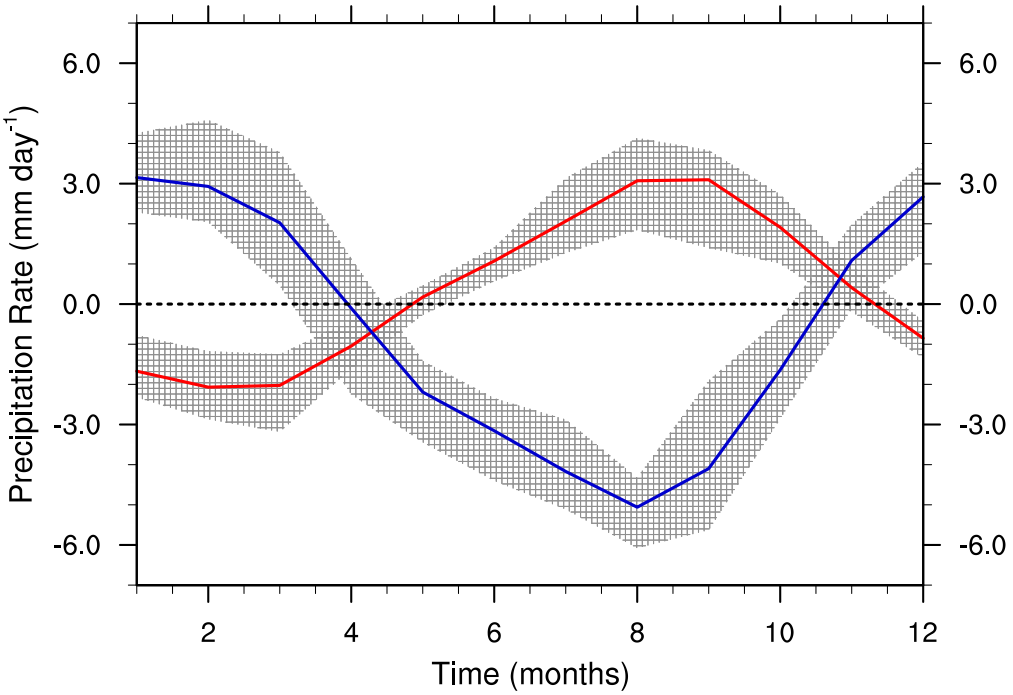

460 Figure 1: Multi-model mean seasonal cycle of the precipitation difference as a function of
461 time between experiments (MH-PI) for the 10 PMIP3 models (listed in Table 1) over land
462 (red) and ocean (blue). Shading indicates the model spread. Curves are scaled by the
463 percentage of land and ocean in the tropics.

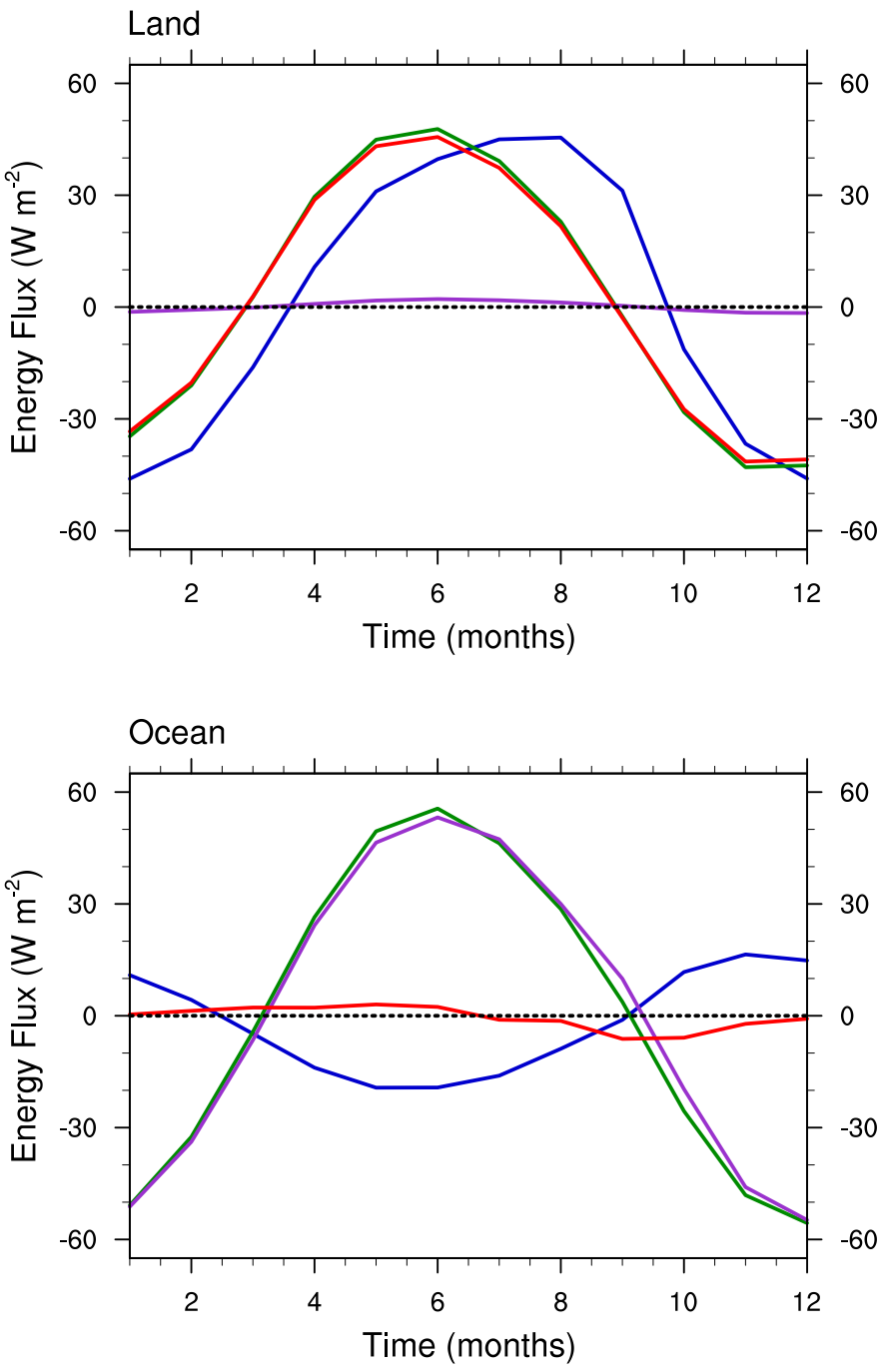

464 Figure 2: Seasonal cycle of the difference (SS-WS) in tropical-mean (30°N to 30°S)
465 precipitation (blue), net TOA radiation (green), net surface energy fluxes (purple), and
466 MSE flux divergence (red) as a function of time over land and ocean for GFDL-CM2.1.

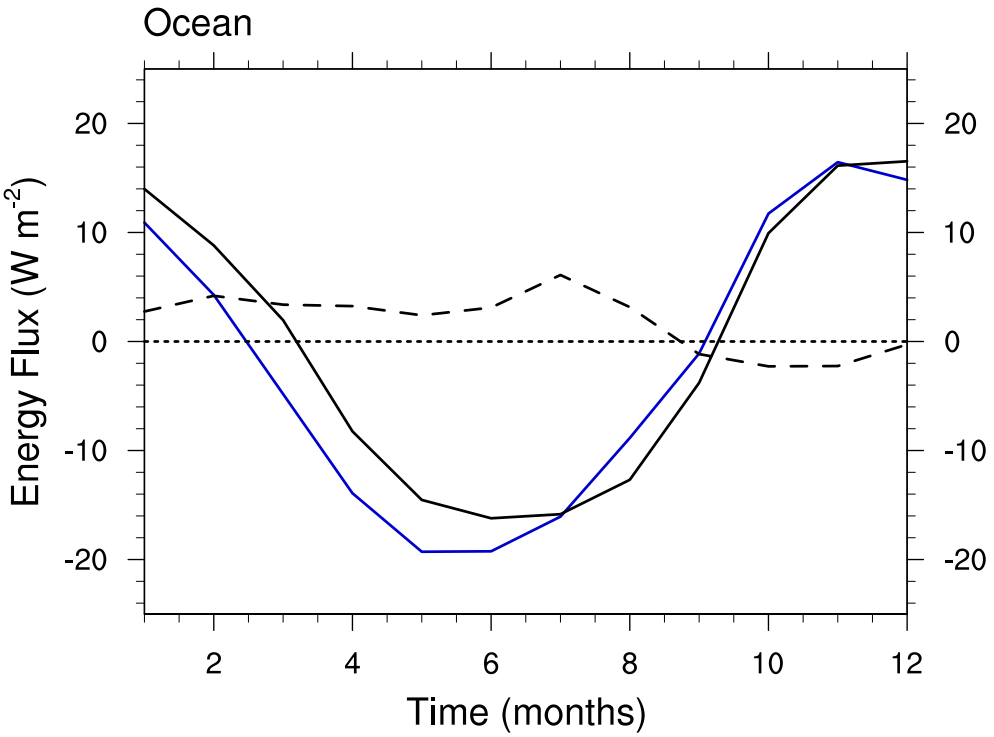

467 Figure 3: Seasonal cycle of the difference (SS-WS) in tropical-mean (30°N to 30°S)
468 precipitation (blue) and moisture flux convergence broken down into circulation changes
469 (solid) and specific humidity changes (dashed) as a function of time over ocean for
470 GFDL-CM2.1.

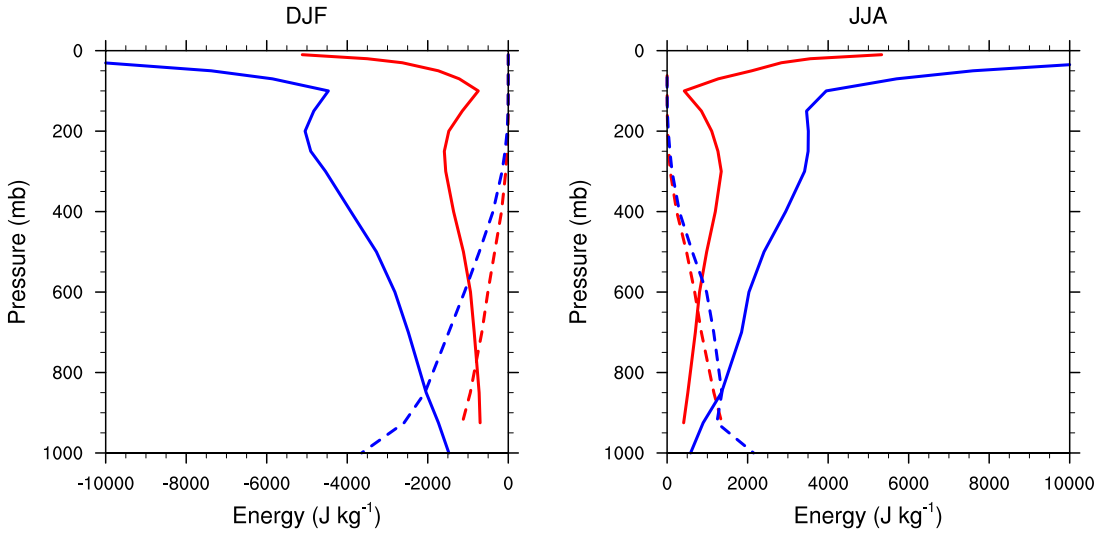

471 Figure 4: Vertical profile of the difference (SS-WS) in tropical-mean (30°N to 30°S) dry
472 (solid) and latent (dashed) energy as a function of pressure over land (red) and ocean
473 (blue) for GFDL-CM2.1. Curves are scaled by the percentage of land and ocean in the
474 tropics.